

Nanoscale

Accepted Manuscript



This is an *Accepted Manuscript*, which has been through the Royal Society of Chemistry peer review process and has been accepted for publication.

Accepted Manuscripts are published online shortly after acceptance, before technical editing, formatting and proof reading. Using this free service, authors can make their results available to the community, in citable form, before we publish the edited article. We will replace this *Accepted Manuscript* with the edited and formatted *Advance Article* as soon as it is available.

You can find more information about *Accepted Manuscripts* in the [Information for Authors](#).

Please note that technical editing may introduce minor changes to the text and/or graphics, which may alter content. The journal's standard [Terms & Conditions](#) and the [Ethical guidelines](#) still apply. In no event shall the Royal Society of Chemistry be held responsible for any errors or omissions in this *Accepted Manuscript* or any consequences arising from the use of any information it contains.

PAPER

Point-of-care Detection and Real-time Monitoring of Intravenously Delivered Drugs via Tubing with an Integrated SERS Sensor

Cite this: DOI: 10.1039/x0xx00000x

Hsin-Yu Wu^a and Brian T. Cunningham^{a,b,*}Received 00th January 2013,
Accepted 00th January 2013

DOI: 10.1039/x0xx00000x

www.rsc.org/

We demonstrate an approach for detection, identification, and kinetic monitoring of drugs flowing within tubing, through the use of a plasmonic nanodome array (PNA) surface. The PNA structures are fabricated using a low-cost nanoreplica molding process upon a flexible plastic substrate that is subsequently integrated with a flow cell that connects in series with ordinary intravenous (IV) drug delivery tubing. To investigate the potential clinical applications for point-of-care detection and real-time monitoring, we perform SERS detection of ten pharmaceutical compounds (hydrocodone, levorphanol, morphine, oxycodone, methadone, phenobarbital, dopamine, diltiazem, promethazine, and mitoxantrone). We demonstrate dose-dependent SERS signal magnitude, resulting in detection limits (ng/ml) well below typical administered dosages (mg/ml). Further, we show that the detected drugs are not permanently attached to the PNA surface, and thus our approach is capable of performing continuous monitoring of drug delivery as materials flow through IV tubing that is connected in series with the sensor. Finally, we demonstrate the potential co-detection of multiple drugs when they are mixed together, and show excellent reproducibility and stability of SERS measurements for periods extending at least five days. The capabilities reported here demonstrate the potential to use PNA SERS surfaces for enhancing the safety of IV drug delivery.

Introduction

Intravenous (IV) therapy is a commonly used method for delivery of liquid-based medications and nutrients to a patient's body in a wide range of clinical settings. Despite the adoption of sophisticated multi-drug pump systems, and quality control efforts that seek to consistently match the prescribed medications with those that are actually delivered to the patient, IV drug delivery remains highly vulnerable to error. Medication errors associated with IV-delivered drugs include incorrect dosage, substitution of one drug for another, co-delivery of incompatible drugs, and infusion of a drug that was not actually prescribed. It has been reported recently that up to 61% of all life-threatening errors during hospitalization are associated with IV drug therapy.¹ Thus, a primary focus of hospitals' medication safety efforts will be upon the prevention of IV medication administration errors, particularly those involving continuous IV drug infusions.² Although current computerized IV infusion safety systems ("smart pumps") help reduce traditional medication errors through programming and calculating dose and delivery rates, such safeguards cannot recognize drugs in an IV line.³ The ability to continuously monitor the contents and concentrations within an

IV line would offer an additional layer of error-checking for minimizing the occurrence of medication errors.

Optical detection techniques, such as fluorescence, infrared absorption, and Raman scattering, are ideal candidates for this task because they are nondestructive, and can be performed without making physical contact to the contents of IV tubing. Although the use of fluorescent tags to detect nonfluorescent target molecules has numerous biomedical applications,^{4,6} it is not permissible to introduce fluorescent dyes into liquid-based medications that are being delivered to the patient's body. Infrared absorption spectroscopy and Raman scattering are label-free detection methods, and thus do not require the use of additional chemical reagents. Nevertheless, the strong absorption cross section of water within the infrared wavelength region significantly interferes with the absorption efficiency of drugs within aqueous media. However, water has a very weak Raman cross section, opening up the possibility for using Raman spectroscopy. Raman scattering provides several advantages over infrared absorption, including inherently narrower bandwidth peaks, and the ability to more specifically identify chemical species by their unique scattering signatures. Unfortunately, Raman scattering cross sections are 12-14 orders of magnitude smaller than fluorescence cross sections of typical molecules, and consequently only one ten millionth of all

incident photons are converted into Raman photons.⁷ As an extremely inefficient process, Raman scattering ordinarily requires a large ensemble of participating molecules along with a high power laser and long acquisition time to produce a measurable signal. This issue has been addressed through the development of surface-enhanced Raman scattering (SERS).⁸⁻¹⁰ SERS is a vibrational spectroscopy technique for rapidly determining chemical identity and structural information from small numbers of molecules in close vicinity to metallic nanostructured surfaces that support regions of intense electromagnetic (EM) field enhancements generated by the excitation of localized surface plasmon-polariton resonances (LSPR). It is this highly localized EM field enhancement at SERS-active sites (referred to as “hot spots”) that cause the strongly enhanced excitation of Raman vibrational modes of adsorbed molecules. Therefore, SERS allows for highly sensitive structural detection of low-concentration analytes with substantially less laser power and shorter detection times than Raman scattering.

Numerous approaches have been demonstrated for producing SERS-active substrates. The most effective of these operate through the incorporation of a periodic metallic nanostructure that is capable of tailoring the LSPR wavelength to the laser excitation wavelength, which in turn couples its electromagnetic field into 10-20 nm dielectric air gaps.¹¹⁻¹⁴ While the intensity of electric field within the nm-scale gap may be up to several thousand times greater than that of the incident illumination source, the field enhancement only occurs within a small fraction of the total surface area. Therefore, SERS scattering signals are only observed for the small fraction of molecules within the enhanced field volume. A high density of hot spots, combined with a high electric field enhancement factor within each hot spot, is important for obtaining a high “average” SERS enhancement factor, representing the most important performance parameter for measurements obtained from a practical system.¹⁵⁻¹⁷

Due to the combined requirements for nm-level precision fabrication and low cost manufacturing for single-use disposable applications, we recently developed a plastic-based approach for fabricating dense arrays of metallic domes.¹⁸ Plasmonic nanodome array (PNA) substrates are produced using a nanoreplica molding technique to form arrays of polymer cylinders, followed by a two-step thin film deposition process to convert the cylinders to rounded domes with controllable and uniform 10-20 nm gaps between adjacent domes. PNA surfaces with an air superstrate were demonstrated to exhibit a spatially averaged SERS enhancement factor (EF) of 8.51×10^7 .¹⁸ In this study, the PNA surfaces are designed specifically for operation with the surface exposed to an aqueous medium through adjustment of thicknesses of the SiO₂ and gold films to tailor the spectral position of the LSPR for $\lambda = 785$ -nm laser excitation.

In this work, we explore the clinical potential of SERS-active PNA surface for identification and verification of the chemical contents of a fluid in an IV line as a means to enhance the safety of IV drug delivery systems. A PNA surface integrated with a miniature plastic flow cell that operates in series with ordinary tubing is used as an in-line SERS sensor for point-of-care detection and real-time monitoring of IV-delivered drugs. We demonstrate SERS detection of ten pharmaceutical compounds, and demonstrate (using four of the ten drugs) that the magnitude of the SERS signal is dependent upon the drug concentration. Kinetic characterization of the SERS signal is used to demonstrate that drug molecules are not

permanently captured by the PNA surface, enabling measurements to be gathered over extended time periods during which the drug concentration may either increase or decrease. Using combined flow of promethazine/mitoxantrone as an example, we demonstrate that multiple drugs present in combination results in a superposition of their SERS spectra, as expected. Finally, we demonstrate that the PNA structure provides reproducible SERS signals over time periods extending up to five days.

Experimental section

Fabrication of PNA substrates

A schematic diagram of the nanoreplica molding process utilized to fabricate the PNA is shown in Fig. S1 in the Electronic Supplementary Information (ESI†).

LSPR reflection measurements

Prior to reflection measurement, a water droplet (10 μ L) was hand-spotted onto the PNA surface and then covered with a cover glass. Far-field reflection measurements of the PNA exposed to water were conducted using an inverted microscope (Axio Observer D1, Carl Zeiss, Inc.) equipped with a 100 W halogen light source. The incident light was focused onto the PNA surface via a 10 \times objective (NA = 0.25) and the reflected light was coupled to a visible and near-infrared (VIS-NIR) spectrometer (Control Development, Inc.) through an optical fiber. All reflection spectra were collected against a mirror-like Au film over microscope glass slide as the reference.

Flow cell with an integrated PNA SERS substrate

The flow cell was made of an optically clear resin (WaterClear Ultra 01122, DSM Somos), fabricated by a stereolithography system (Viper SLA system, 3D Systems). A cut PNA coupon with a square area of 1 cm² was inserted into the middle slit of the flow cell and sealed by UV-cured adhesive (Addison Clear Wave). Both top and bottom surfaces of the flow cell were sealed by attaching No. 1 glass coverslips (12 \times 24 mm) using the same adhesive. The cross-sectional area of the inlet and outlet was 3.5 \times 1 mm. The distance between the top glass window and the PNA surface was \sim 1.5 mm. The cylindrical openings at the two ends of the flow cell were tapped and screwed in with barbed male threaded adapters (10-32 UNF \times 1/8” ID, Cole-Parmer) connected to biomedical tubing (1/8” ID \times 3/16” OD \times 1/32” Wall, TYGON R-3603). Please refer to Fig. S2 in the ESI† for fabrication details of the flow cell.

Detection instrument and data analyses

SERS measurements were carried out using a Renishaw inVia Raman microscope equipped with a NIR diode laser ($\lambda_{\text{exc}} = 785$ nm) and a 50 \times objective (NA = 0.5) with a working distance of 8.2 mm. Under the activation of an excitation pinhole that improves the beam profile and spatial resolution, the measured NIR diode laser power at the exit of the objective is 512 μ W for concentration series and mixture solutions experiments. The measured NIR diode laser power at the exit of the objective is 5.9 mW for kinetic experiments. The back-scattered photons were collected by the same objective lens and sent through a holographic notch filter and a Peltier-cooled CCD detector to acquire SERS spectra with a spectral resolution of \sim 0.5 cm⁻¹. All measurement data were gathered using a linearly polarized

laser beam oriented in the x -axis with an integration time of 10 s for concentration series and mixture solutions experiments, and 5 s for kinetic experiments. Raw spectra were smoothed using the Savitsky–Golay method with a third-order polynomial and window size of 9. The slowly varying background of the processed spectra was removed by subtracting the processed reference spectrum taken from the blank solution (DI water). This method greatly reduced varying background levels with minimum effect on the net SERS peaks. All calibration curves shown in this work were fit using Hill equation with $n = 1$, which is equivalent to the Langmuir equation.

Experimental procedures

Analytical grade drugs used in this study were purchased from Sigma-Aldrich. For concentration series measurements, each drug was prepared in DI water at five different concentrations. Prior to the SERS measurements, SERS spectra of a blank solution were first taken as references at five different recorded locations on the PNA surface, followed by emptying DI water from the PNA surface. The lowest concentration analyte solution was introduced onto the PNA surface and then SERS measurements were taken on the same locations as the measured reference spectra. After the measurements, the analyte solution was emptied out, followed by rinsing with DI water three times before beginning the next higher analyte concentration measurement. Measurements were taken in a static condition without flow with an integration time of 10 s. For mixture solutions of promethazine and mitoxantrone, test samples were prepared in four concentration combinations in DI water: 12.5 mg/ml, 1.95 μ g/ml; 6.25 mg/ml, 1.95 μ g/ml; 50 μ g/ml, 3.91 μ g/ml; 50 μ g/ml, 1.95 μ g/ml for promethazine and mitoxantrone, respectively. The experimental procedure was identical to that mentioned in the concentration series measurements. For the kinetic on/off measurements, two separate programmable syringe pumps (PHD 2000/4400, Harvard Apparatus) were used to alternately infuse DI water (blank) and the analyte solution into their individual biomedical tubing at 50 s intervals over 650 s. The solutions were pumped through the tubing at a flow rate of 5 ml/min. A three-way stopcock connected to the biomedical tubing was used as a switching valve, which was synchronized with the syringe pumps, to alternate the flowing blank and sample streams into a third section of tubing connected to the inlet of flow cell. SERS spectra were captured every 5 s with an integration time of 5 s.

Results and discussion

In-line SERS sensor

For SERS surfaces to be adopted for single-use disposable point-of-care diagnostic applications, the structure must be inexpensively manufacturable over large surface areas while simultaneously providing a reliable and reproducible enhancement factor (EF). The PNA structure used in this work is produced on a flexible plastic substrate by a low-cost, large-area, and high-throughput nanoreplica molding technique, which provides a spatially averaged SERS EF of 8.51×10^7 with a surface density of $6.25 \times 10^6 \text{ mm}^{-2}$ hot spots¹⁸. Fig. 1(a) shows a photograph of the completed PNA structure on a flexible polyester substrate over a $100 \times 75 \text{ mm}^2$ surface area. Gold was chosen as the plasmonic material because it is less susceptible than silver to oxidation, which causes degradation of EF, which is a particular concern for long-term detection within aqueous media. Fig. 1(b) shows scanning electron

microscope (SEM) images of the fabricated PNA structure with square lattice symmetry (period = 400 nm). The sensor is incorporated into a miniature flow cell made from optically clear resin, as shown in Fig. 1(c). Fig. 1(d) illustrates an in-line SERS sensor where two cylindrical openings at the ends of the SERS sensor are connected in series with biomedical tubing and the excitation laser ($\lambda_{\text{exc}} = 785 \text{ nm}$) is focused on the PNA surface by a $50\times$ objective with NA = 0.5. The SERS sensor provides label-free identification/detection of analytes due to diffusion of the analyte molecules into the SERS-active regions without immobilization of capture probe molecules on the sensor surface.

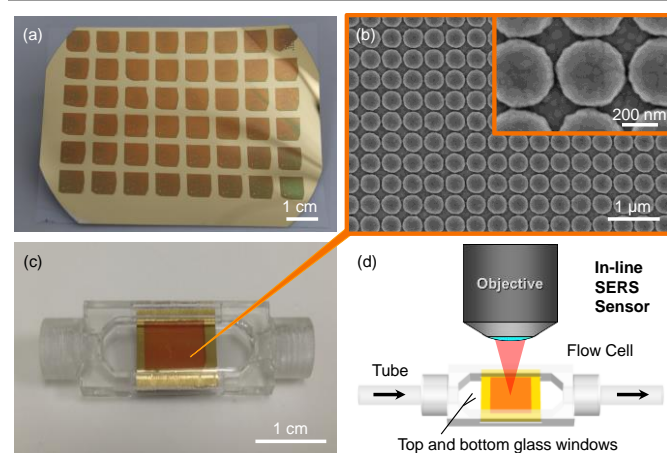


Fig. 1 (a) Image of the PNA surface fabricated on a flexible polymer sheet. (b) SEM image of the completed PNA surface. Inset: close-up SEM image of the PNA surface with measured inter-dome separation distance of 15–20 nm. (c) Image of the SERS sensor assembled by incorporation of the flexible PNA substrate into a plastic flow cell. (d) Schematic of an in-line SERS sensor where two cylindrical openings at the ends of the SERS sensor are connected in series with biomedical tubing and a 785-nm laser focused on the PNA surface by a $50\times$ objective.

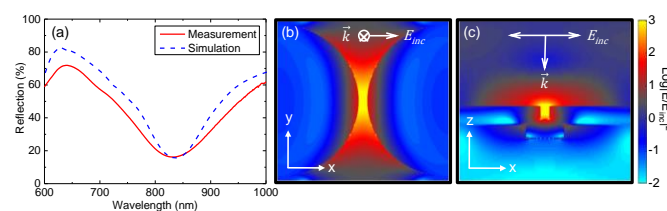


Fig. 2 (a) Measured and FDTD-computed reflection spectra of the PNA surface exposed to water. (b) Top and (c) cross-sectional views of the spatial electric-field intensity enhancement profiles of one unit cell volume of the PNA for the LSPR resonance ($\lambda_{\text{LSPR}} = 832 \text{ nm}$). E_{inc} indicates the orientation of the incident electric field vector of a monochromatic plane wave.

In addition to analyte molecules spatially positioned within the hot-spot regions, the spectral location of the LSPR is also important because it has been demonstrated that the maximum SERS EF occurs when the LSPR wavelength (λ_{LSPR}) lies between the excitation wavelength (λ_{exc}) and Raman scattered wavelength (λ_{RS}) because LSPR is relatively broad and hence both the incident and the Raman scattered photons can be simultaneously and strongly enhanced.¹⁹ Fig. 2(a) shows experimental and simulated reflection spectra of the PNA surface covered in water. Detailed simulation parameters are summarized in the ESI†. The resonance spectral wavelength obtained from experimental measurement correlates well with the wavelength predicted by computer simulation. The

discrepancy in the linewidth between experiment and simulation can be attributed to the structural aspects such as surface roughness and feature size variations, and extra losses in the metal due to increased surface scattering and grain surface effects of the underlying SiO₂ film, which are not taken into account in the simulation. Since the PNA substrate coated with a 180 nm gold film is not optically transparent, the reflection minimum wavelength ($\lambda_{\text{min}} = 832$ nm) was used to locate the LSPR extinction maximum wavelength (λ_{LSPR}). Moreover, the dominant SERS intensity peaks for IV-delivered drugs used in this work are situated between 1000 and 1500 cm⁻¹ shift, corresponding to Raman scattered wavelength (λ_{RS}) ranging from 852 to 890 nm. Consequently, measured λ_{LSPR} of 832 nm meets the criteria of the maximum SERS EF. Fig. 2(b) and (c) show top and cross-sectional views of the spatial electric-field intensity enhancement distributions associated with the dipole LSPR mode.¹⁸ The most intense electric-field intensity (the hot spot) is confined within the gap between adjacent nanodomains, depicted as the yellow region.

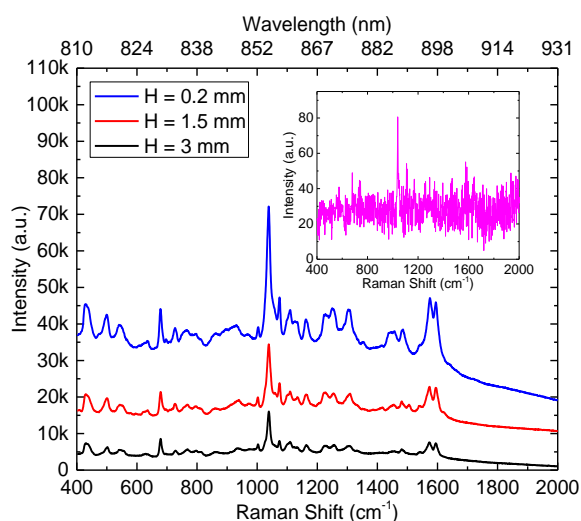


Fig. 3 SERS spectra of 25 mg/ml promethazine solution for SERS sensors with varying chamber heights (H). Primary SERS intensity peak for promethazine can be observed at 1037 cm⁻¹. The inset represents the Raman spectrum of 25 mg/ml promethazine solution, acquired when the laser was focused on a uniform non-nanostructured gold surface.

In order to investigate the effect of the chamber height of the flow cell on the SERS intensity, SERS measurements were carried out on flow cells of three different depths filled with 25 mg/ml promethazine solution, representing a clinically relevant concentration typically delivered to patients. Fig. 3 compares the SERS spectra of 25 mg/ml promethazine solutions gathered from the three different chamber heights ($H = 0.2$, 1.5, and 3 mm). The SERS spectra of promethazine reveals a dominant SERS intensity peak at 1037 cm⁻¹, due to the breathing mode of the aromatic rings, a small peak at 677 cm⁻¹, which can be assigned to a C_{ring}-S stretching mode, as well as two minor peaks at 1573 and 1593 cm⁻¹, which can be assigned to the aromatic C=C stretching modes.²⁰ The inset shows the Raman spectrum of 25 mg/ml promethazine solution, acquired when the laser was focused on a uniform gold surface without nanostructures. It should be pointed out that the measured Raman signal was largely collected from the drug molecules within the laser probe volume with the same laser power of 512 μ W and integration time of 10 s as SERS measurements. When

the laser was focused on a uniform gold surface without nanostructures, the focused beam waist of the laser extends for ~ 22 μ m in the direction perpendicular to the surface, which is very small compared to H (ESI[†]). Thus, as expected, identical Raman intensities are obtained regardless of the size of the flow cell height. After background subtraction, the ratios of dominant SERS intensities to Raman intensity at 1037 cm⁻¹ are 666, 300, and 192 for $H = 0.2$, 1.5 and 3 mm, respectively. As shown in Fig. 3, SERS intensity decreases with increasing chamber height, which can be attributed to less efficient focusing of the excitation laser spot when it passes through increased depth of the liquid sample, which in turn results in a large decrease in measured SERS intensity, which is proportional to the square of the laser power coupled into the PNA surface. Thus, obtaining greater SERS intensity favors the selection of a shallow flow channel height, but at the expense of a chamber volume that may not accommodate clinical flow rates. Therefore, in this work, the PNA substrate is positioned in the center of a flow cell with 3.0 mm height, allowing the flow to bifurcate above and below the active PNA surface. The distance between the top glass window and the PNA surface is ~ 1.5 mm while at the same time enabling flow rates of 0.1 – 5 ml/min to be used without pressure buildup within the flow cell.

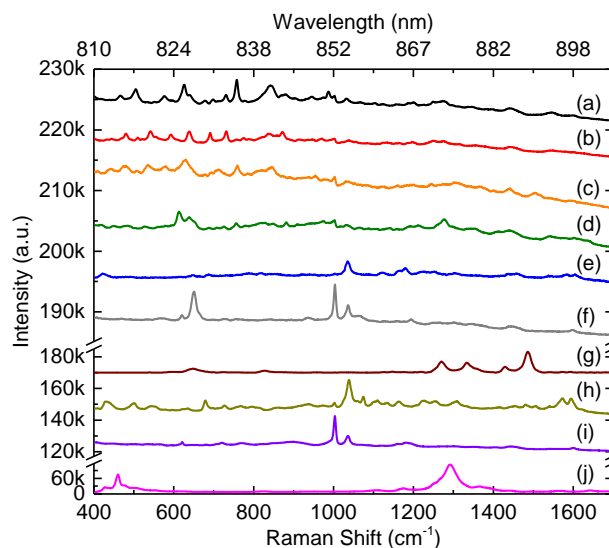


Fig. 4 SERS spectra of ten pharmaceutical drugs measured at concentrations used in clinical drug delivery: (a) hydrocodone (0.5 mg/ml), (b) levorphanol (2 mg/ml), (c) morphine (5 mg/ml), (d) oxycodone (20 mg/ml), (e) diltiazem (1 mg/ml), (f) phenobarbital (65 mg/ml), (g) dopamine (1.6 mg/ml), (h) promethazine (25 mg/ml), (i) methadone (10 mg/ml), and (j) mitoxantrone (2 mg/ml). All spectra were gathered by a 785-nm laser with an output power of 512 μ W and an integration time of 10 s. For clarity and comparison, SERS spectra are vertically offset.

Detection of pharmaceutical drugs

Fig. 4 shows the measured SERS spectra of ten pharmaceutical drugs at typical clinically delivered concentrations. They are opioid pain medications (hydrocodone (0.5 mg/ml), levorphanol (2 mg/ml), morphine (5 mg/ml), oxycodone (20 mg/ml), methadone (10 mg/ml) and phenobarbital (65 mg/ml)), medications for the prevention and/or treatment of renal dysfunction (dopamine (1.6 mg/ml) and diltiazem (1 mg/ml)), and sedative/pain medications (promethazine (25 mg/ml) and mitoxantrone (2 mg/ml)). Each drug was prepared in water, and

SERS spectra shown for all of the drugs were averaged over five different locations on the sensor surface. The most prominent SERS bands in the measured spectra are in agreement with those previously reported by other groups.^{21, 22} We chose four representative drugs (dopamine, diltiazem, promethazine and mitoxantrone) as model materials to perform dose-dependent detection of low-concentration analytes to explore detection limits. In addition, we performed kinetic detection of two representative drugs (promethazine and mitoxantrone) under flow, to investigate the ability to detect changes of drug concentration, and to observe the rate at which drugs are flushed into and out of the flow cell.

Dose-response characterization and detection limits

A decrease in cardiac output in the early stage after cardiac surgery is a frequent cause of acute renal failure. Dopamine, a natriuretic hormone, is used extensively to increase renal blood flow and raise glomerular filtration rate, which cause increased diuresis that protects against acute renal failure in oliguric patients who are in shock or heart failure.^{23, 24} Dopamine is usually administered by continuous IV infusion, and most common concentrations in IV bags are 0.8, 1.6, and 3.2 mg/ml. High dosage can cause ventricular arrhythmias, hypertension, tachycardia, and peripheral vasoconstriction.²⁵ Fig. 5(a) plots the SERS spectra for dopamine solutions of varying concentrations ranging from 0.781 to 200 $\mu\text{g/ml}$. It is obvious that the SERS spectra of dopamine solutions reveal several characteristic SERS intensity peaks located at 649, 828, 1270, 1334, 1430, and 1486 cm^{-1} . Two prominent peaks at 1486 and 1270 cm^{-1} were assigned to phenyl C=C and phenolic C-O stretching modes, respectively.^{26, 27} The inset shows a calibration curve of averaged SERS intensity measured at 1486 cm^{-1} as a function of dopamine concentration with error bars indicating ± 1 standard deviation measured from five different recorded locations on the sensor surface ($N = 5$). The data points were then fit using a Langmuir equation with a correlation coefficient (R^2) value of 0.999.

Diltiazem, a calcium channel blocking agent, is often used in the treatment of hypertension, angina pectoris, and some types of arrhythmia.^{28, 29} Besides its cardiac effects, diltiazem has been used to treat or prevent acute kidney injury associated with cardiovascular surgery and renal transplantation by enhancing glomerular filtration rate, diuresis, and natriuresis.^{23, 24} The maximum recommended concentrations for continuous IV infusion and IV push are respectively 1 and 5 mg/ml, and events observed following diltiazem overdose included bradycardia, hypotension, asystole, and AV block.³⁰ Fig. 5(b) displays the SERS spectra for diltiazem solutions of varying concentrations ranging from 0.977 to 250 $\mu\text{g/ml}$. The SERS spectra of diltiazem solutions exhibit a dominant SERS intensity peak located at 1033 cm^{-1} , which can be assigned to the ring breathing mode. Using the dominant peak intensity value for quantitative analysis of diltiazem, the inset presents a calibration curve of the averaged SERS intensity as a function of diltiazem concentration with error bars representing ± 1 standard deviation measured from five different recorded locations on the sensor surface ($N = 5$). The data points in the inset were fit using a Langmuir equation with an R^2 value of 0.993.

From the calibration curves shown in the insets of Fig. 5(a) and (b), we can clearly see that at low concentration range the SERS intensity increases linearly with concentration, while at higher concentration range the SERS intensity increases slowly as the hot spot nanogap sites on the PNA surface gradually

become fully occupied. For each drug, the limit of detection (LOD) is defined as the concentration at which the SERS intensity value is equal to three times the standard deviation (σ) of five blank intensities at the dominant peak (1487 cm^{-1} for dopamine and 1033 cm^{-1} for diltiazem). Therefore, by substituting three standard deviations (3σ) into the correspondingly fit Langmuir equation, the LODs were calculated to be 731 ng/ml for dopamine and 455 ng/ml for diltiazem. The results suggest that the PNA substrate is capable of rapidly identifying dopamine and diltiazem compounds and quantitatively detecting the changes in their IV solution concentration, hence preventing hazards associated with overdose, since the detection limits of the PNA substrate are well below their individual maximum allowed IV-delivered concentrations. While the diltiazem detection data shown here was obtained with the drug dissolved in DI water, in the clinic it can be administered in phosphate buffered saline (PBS). We have verified that PBS does not generate its own SERS signal. Additional information is given in the ESI†.

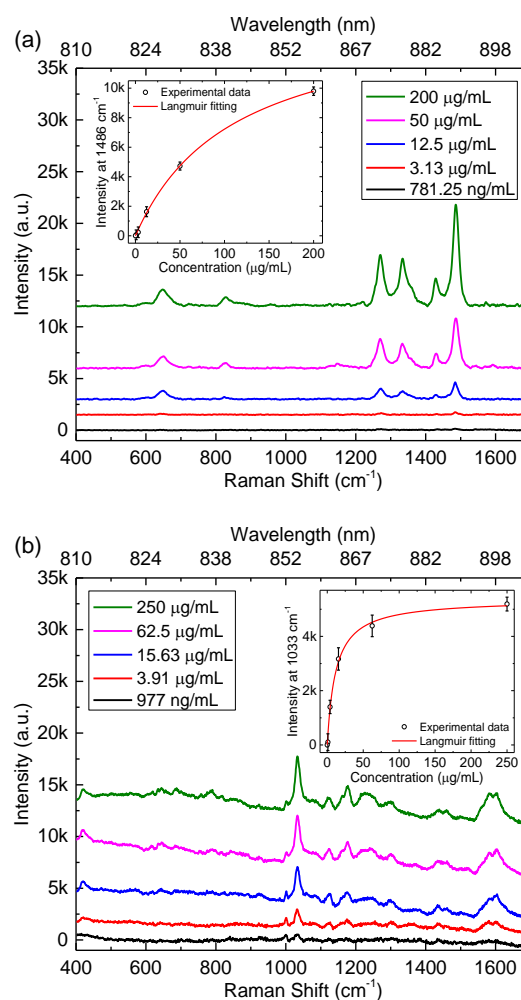


Fig. 5 SERS spectra of (a) dopamine and (b) diltiazem solutions at various concentrations. Individual primary SERS intensity peak can be observed at 1486 cm^{-1} for dopamine compound and 1033 cm^{-1} for diltiazem compound, corresponding to the phenyl C=C and C-O stretching modes, respectively. The inset in the figure represents a calibration curve of the averaged SERS intensity measured at (a) 1486 cm^{-1} and (b) 1033 cm^{-1} as a function of analyte concentration. The error bars indicate ± 1 standard deviation measured from five different recorded locations on the sensor surface ($N = 5$). The red curve shows the Langmuir equation fit to the experimental data.

Promethazine, a phenothiazine derivative, is a commonly used injectable medicine that provides clinically useful antihistamine, antiemetic, and sedative effects. Promethazine is often used to treat and relieve some types of allergy or allergic reactions and prevent and reduce nausea, vomiting, and motion sickness.^{31, 32} When administered intravenously, promethazine should be given in a concentration no greater than 25 mg/ml. Overdose can cause severe tissue injury, including gangrene, requiring fasciotomy, skin graft, and/or amputation.³³ Fig. 6(a) plots the SERS spectra for promethazine solutions of varying concentrations ranging from 0.763 to 195.31 $\mu\text{g/ml}$. The SERS spectra of promethazine solutions reveals a primary SERS intensity peak located at 1037 cm^{-1} corresponding to the ring breathing mode of the aromatic rings.²⁰ Using the primary peak intensity at 1037 cm^{-1} for quantitative analysis of promethazine, the inset shows a calibration curve of the averaged SERS intensity as a function of promethazine concentration with error bars indicating ± 1 standard deviation measured from five different recorded locations on the sensor surface ($N = 5$). Langmuir model offered a good fit for the experimental data with an R^2 value of 0.999.

Mitoxantrone is an anti-cancer (antineoplastic or cytotoxic) chemotherapy drug. It is used to clinically treat certain types of cancer such as metastatic breast cancer, acute myeloid leukemia, and non-Hodgkin's lymphoma.³⁴ Besides being used as antineoplastic agent, mitoxantrone is also applied for therapy of multiple sclerosis.²⁰ For mitoxantrone IV injection, the recommended dosage is 2 mg/ml, and congestive heart failure, tachycardia, and severe myelosuppression will occur when used in high doses. Fig. 6(b) displays the SERS spectra for mitoxantrone solutions of varying concentrations ranging from 0.061 to 15.63 $\mu\text{g/ml}$. The SERS spectra of mitoxantrone solutions exhibit two prominent SERS intensity peaks located at 461 and 1292 cm^{-1} . The 1292 cm^{-1} band is the most intense feature in the spectra and was assigned to the ring stretching mode coupled with C–O motions.³⁵ The inset presents a calibration curve of the average SERS intensity measured at 1292 cm^{-1} with error bars representing ± 1 standard deviation measured from five different recorded locations on sensor surface ($N = 5$). A good fit using a Langmuir equation with an R^2 value of 0.998 was obtained.

The calibration curve presented in the inset of Fig. 6(a) shows the similar trend as with the experiments of dopamine and diltiazem, while in the case of mitoxantrone, the calibration curve (inset of Fig. 6(b)) exhibits a nearly linear response because the analyte concentration is within the dynamic range of the PNA substrate. Furthermore, mitoxantrone has an absorption maximum near a wavelength of 660 nm, allowing an excitation source such as a HeNe laser to excite resonant vibration modes.³⁶ Such surface-enhanced resonance Raman scattering (SERRS) is capable of further amplifying Raman scattering signals by $10^3 - 10^5$ times compared with nonresonant SERS in our study since the resonance Raman effect usually does not exist in the NIR region.^{37, 38} Based on the fit Langmuir equation and three standard deviation (3σ) threshold as the sensor readout resolution, the LODs were calculated to be 638 ng/ml for promethazine and 18.6 ng/ml for mitoxantrone. Again, the obtained LODs are well below their individual maximum allowed IV-delivered concentrations, suggesting that the PNA substrate could be used to identify promethazine and mitoxantrone compounds and quantitatively detect the changes in their IV solution concentration in order to prevent the occurrence of medication errors.

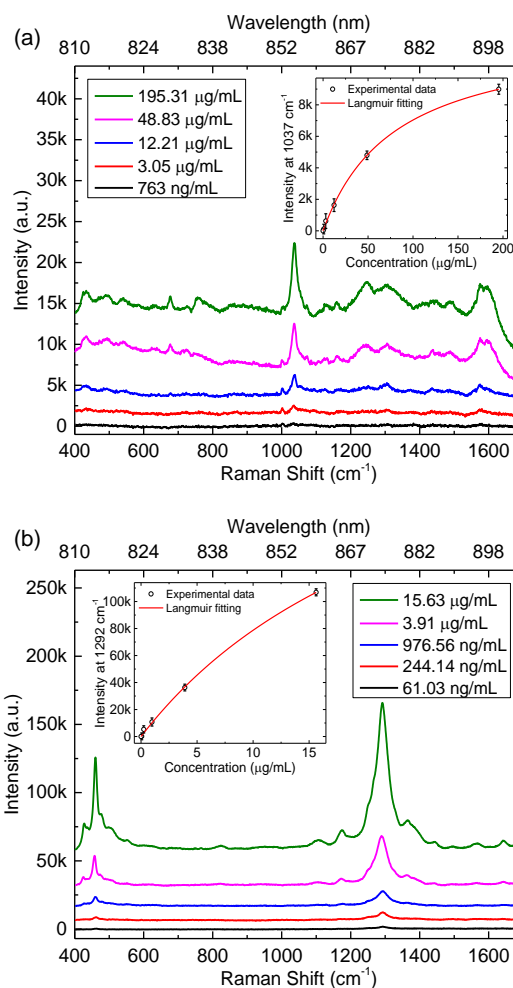


Fig. 6 SERS spectra of (a) promethazine and (b) mitoxantrone solutions at various concentrations. Individual primary SERS intensity peak can be observed at 1037 cm^{-1} for promethazine compound and 1292 cm^{-1} for mitoxantrone compound, corresponding to the ring-breathing mode of the aromatic rings and the ring stretching mode coupled with C–O motions, respectively. The inset in the figure represents a calibration curve of the averaged SERS intensity measured at (a) 1037 cm^{-1} and (b) 1292 cm^{-1} as a function of analyte concentration. The error bars indicate ± 1 standard deviation measured from five different recorded locations on the sensor surface ($N = 5$). The red curve shows the Langmuir equation fit to the experimental data.

It should be noted that the laser power of $512\text{ }\mu\text{W}$, delivered to the sample via $50\times$ objective ($NA = 0.5$), was chosen to avoid the issues such as photodegradation and photobleaching of the analyte. For the Raman setup utilized in the present study, the laser spot size (diameter) and the effective probe length were respectively characterized to be $3.13\text{ }\mu\text{m}$ and $44.86\text{ }\mu\text{m}$. When the laser beam is focused on the surface, the laser probe volume (the detection region) is modeled as a cylinder with a diameter and a height equivalent to the measured laser spot size and half the effective probe length (ESI†). In consequence, under the laser illumination area, the number of hot spots on the PNA surface is ~ 48 according to a single EM hot spot per unit cell area of 400^2 nm^2 , as shown in Fig. 1(b) and 2(b). The overall volume of EM hot spots within the laser spot area is approximately $0.0022\text{ }\mu\text{m}^3$ based on the volume of a single EM hot spot of 45375 nm^3 by assuming that the hot-spot region is bounded by the distance where the enhanced electric intensity decays to $1/e^2$ of its maximum value in FDTD

simulation results. For this reason, only those analytes residing within or in close vicinity to the SERS-active volume of $0.0022 \mu\text{m}^3$, which supports the regions of highly intense EM enhancement associated with LSPR, contribute a predominant portion of the overall measured signal, while analytes far beyond the SERS-active volume but nonetheless within the laser probe volume are largely responsible for the Raman signal although this contribution is very small, as shown in the inset of Fig. 3.

Detection of real-time kinetic drug concentration changes

The ability to continuously monitor concentration fluctuations is essential for SERS sensors to be implemented in the clinical environment. In order to investigate real-time detection capability of SERS sensor, SERS measurements were made with DI water and a $500 \mu\text{g/ml}$ promethazine solution alternately infused through SERS sensor tubing at time intervals of 50 s, with SERS spectra acquired every 5 s with an integration time of 5 s. Fig. 7(a) shows the kinetic sensor response to changes in promethazine concentration by monitoring the SERS intensity at 1037 cm^{-1} as a function of time. Likewise, SERS measurements were made with DI water and a $2 \mu\text{g/ml}$ mitoxantrone solution alternately infused through SERS sensor tubing at 50 s intervals, and SERS spectra were collected using the same measurement interval and integration time. Fig. 7(b) shows the sensor kinetic response to changes in mitoxantrone concentration by monitoring the SERS intensity at 1292 cm^{-1} as a function of time. Although ordinary IV injection rates are relatively low, an infusion rate of 5 ml/min was chosen to facilitate the kinetic experiment and minimize analyte dispersion (diffusion along tubing) that occurs at the interface between different solutions as they are being pumped into the tubing. As a consequence, when the analyte solution is pumped through the SERS sensor flow cell, analyte molecules initially residing in proximity to the PNA surface have an increased probability of diffusing across a stagnant layer and intersecting the hot-spot regions before being swept away from the PNA surface. Conversely, molecules far away from the PNA surface will be swept downstream before they can diffuse very far.

Our detection approach is based upon diffusion of the analyte molecules into the SERS-active regions without the requirement for surface chemistry, making this method suitable for continuous in-line monitoring of IV-delivered drugs, where immobilization of capture probes onto the PNA surface by selective molecule coating is not desirable. As shown in Fig. 7(a), delay in sensor response can be observed due to the diffusion of molecules in the stagnant boundary layer as promethazine solution is pumped through the SERS sensor. By contrast, a rapid response in SERS intensity upon exposure of the sensor to mitoxantrone solution is shown in Fig. 7(b), because mitoxantrone is a highly effective scattering molecule and has higher adsorption affinity to the PNA surface than promethazine.³⁹ Subsequent cycles of high/low drug concentration results in a gradual overall increase in SERS intensity for the first ~4 cycles, followed by establishment of equilibrium values for the highest and lowest SERS intensity. The data in Fig. 7(a) and (b) reveals, after removal of drug from the flow stream, an initial rapid decrease in SERS intensity for ~15 seconds, followed by a more gradual reduction for the next 15-50 seconds. Although the SERS intensity is continuing a downward trend after 50 seconds, the short interval was not sufficient to completely wash the drug from the flow cell or from the sensor surface. We hypothesize the presence of two

simultaneous mechanisms that are responsible for the observed kinetic behavior. First, the rapid decrease of SERS intensity following removal of the drug from the flow stream is the result of fluid replacement within the flow cell, and that after ~15 seconds, given our flow rate (5 ml/min) and the volume of flow cell (462 mm^3), the fluid has been effectively exchanged 6.3 times. The more gradual reduction in SERS intensity for the time period 15-50 seconds after drug removal is partially the result of the stagnant boundary layer at the solid-liquid interface that results in the requirement for diffusion of drugs for a ~1-2 micron distance before they are effectively displaced from the sensor. The potential ability for drug molecules to associate with the gold surface through adsorption may also be responsible for the slow rate of SERS signal decrease.

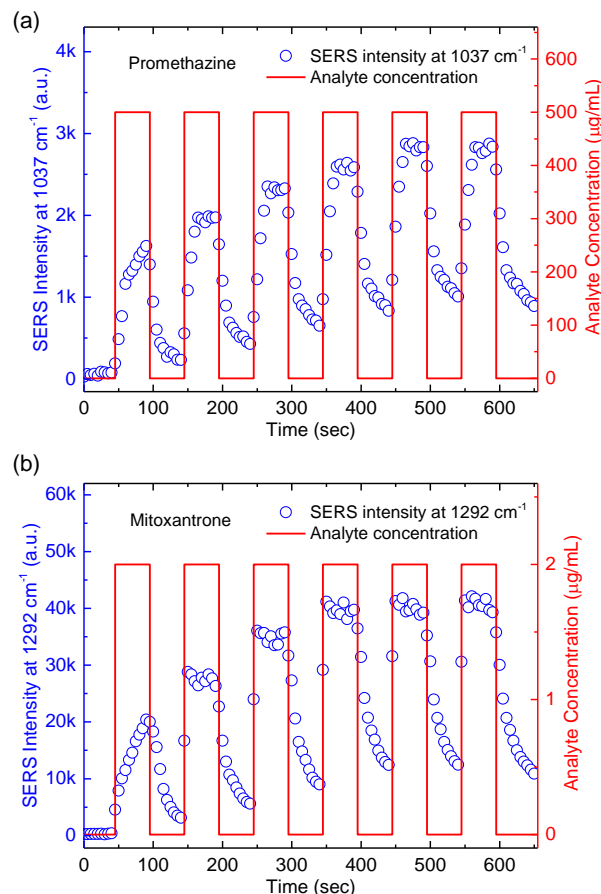


Fig. 7 (a) Kinetic plot of SERS intensity at 1037 cm^{-1} as $500 \mu\text{g/ml}$ promethazine solution and DI water were alternately pumped through the SERS sensor at 50 s intervals. (b) Kinetic plot of SERS intensity at 1292 cm^{-1} as $2 \mu\text{g/ml}$ mitoxantrone solution and DI water were alternately pumped through the SERS sensor at 50 s intervals.

Detection of drug mixtures

SERS offers a capability for simultaneous detection of multiple analytes provided that SERS peaks of analytes of interest have little spectral overlap, which provides a potential benefit for enhanced patient safety when a combination of two or more distinct medications is delivered through an IV line in clinical settings. In order to demonstrate the multiplexed detection capability of the SERS sensor, mixed solutions of promethazine and mitoxantrone at different concentrations were introduced to the PNA surface. Fig. 8 shows the SERS spectra

for four promethazine and mitoxantrone mixtures where individual primary SERS intensity peak for promethazine and mitoxantrone can be readily distinguished at 1037 and 1292 cm^{-1} from the mixtures, and the intensity values for each drug compound were in agreement with the measurements made with single drug solutions. Measurements were taken in sequence from the top to bottom of Fig. 8, where relative changes in the concentrations of two drugs, using the same sensor, shows reduction and elimination of the SERS spectra when the drug concentration is reduced. Drugs appear not to be permanently bound to the sensor surface due to the ability to easily eliminate the SERS signal with a simple wash procedure. While none of the drugs evaluated in our study were found to undergo a chemical reaction with the gold sensor surface, or to permanently adsorb to it, the presence of such a molecule would be capable of displacing other non-binding molecules from the hot spots on the PNA surface, resulting in preferential SERS detection. Thus, the measured SERS intensity is the result of the number of molecules within illuminated hot spots and the molecule's Raman cross section. Detection of weakly-adsorbing or nonadsorbing molecules at low concentration in the presence of chemically reactive or strongly adsorbing molecules will be a challenge for any SERS approach.

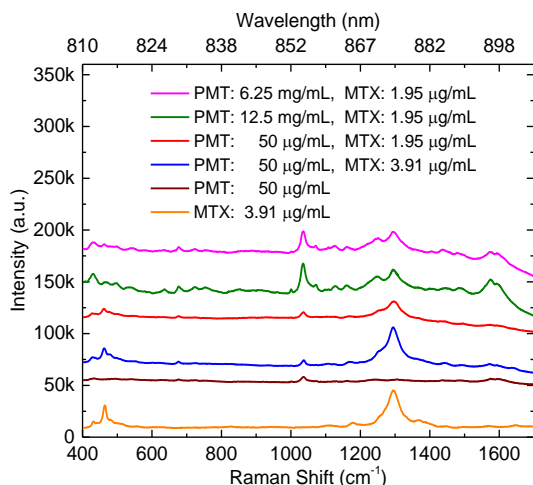


Fig. 8 SERS spectra of promethazine (PMT) and mitoxantrone (MTX) mixtures, PMT, and MTX. Individual primary SERS intensity peaks for both promethazine and mitoxantrone compounds can be identified at 1037 and 1292 cm^{-1} , respectively.

Stability and reproducibility of SERS measurements

The SERS-active PNA surface utilized in this work consists of metal-dielectric thin-film coatings that are anchored over the entire surface of polymer cylinders adhering to the flexible polyester substrate. This robust SERS structure along with a reliable SERS EF plays a significant role in the stability and reproducibility of measurements. In order to study the stability and reproducibility of the SERS sensor, the SERS measurement was conducted on the same locations (three recorded locations on the PNA surface that were 400 μm apart from each other) over a period of 5 days on the SERS sensor filled with 25 mg/ml promethazine solution. The SERS spectra were captured every 24 h from the same locations with an integration time of 10 s after the initial exposure to the promethazine solution. Fig. 9(a) represents the SERS spectra of 25 mg/ml promethazine solution within the SERS sensor for five days after the initial exposure. The inset shows a time course of averaged SERS

intensity measured at 1037 cm^{-1} with error bars indicating ± 1 standard deviation measured from three recorded locations on the PNA surface that were 400 μm apart from each other ($N = 3$). It is obvious that the 1037 cm^{-1} band positions and relative intensities do not vary significantly over the course of 5 days. Moreover, in order to evaluate batch-to-batch reproducibility of the SERS sensor, the same experiment was repeated on a fresh sensor device made from a separate fabrication batch, as shown in Fig. 9(b). The results show that the peak intensity of the 1037 cm^{-1} band remains constant as time progresses, indicating that the PNA surface remains SERS-active and exhibits a robust performance over a period of 5 days.

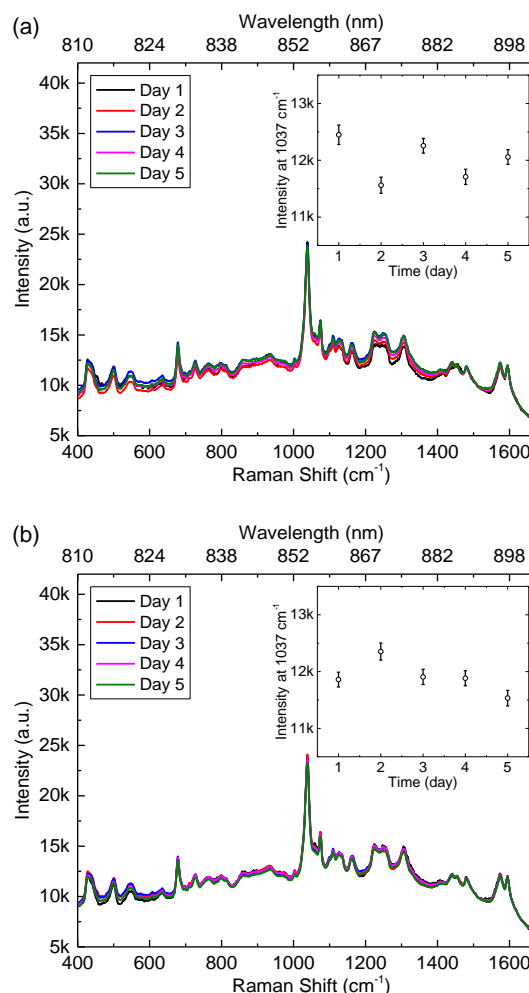


Fig. 9 SERS spectra of 25 mg/ml promethazine solution within (a) the SERS sensor and (b) the SERS sensor made from a separate fabrication batch, up to five days after the initial exposure to the promethazine solution. The inset in the figure represents a time course of averaged SERS intensity measured at 1037 cm^{-1} . The error bars indicate ± 1 standard deviation measured from three recorded locations on the PNA surface that were 400 μm apart from each other on the sensor surface ($N = 3$). All spectra were gathered by a 785-nm laser with an output power of 512 μW and an integration time of 10 s.

Conclusions

We have experimentally demonstrated that an in-line SERS sensor has a great potential for enhanced safety of current smart infusion systems through point-of-care detection and real-time monitoring of IV fluids within biomedical tubing. We have

demonstrated the ability of SERS sensors to quantitatively identify drug compounds and to kinetically monitor changes in drug concentration as well as to simultaneously detect a combination of two drugs. We have showed that the spectral alignment between the LSPR and excitation/Raman scattering together with an appropriate chamber height results in detection limits in the 19 – 731 ng/ml range well below typical drug dosages (mg/ml). Because the nanoreplica molding process used to make PNA substrates is an inexpensive and mass-manufacturing nanofabrication method, and because PNA surfaces with consistent nanogap spacing, and hence reproducible SERS EF, can be fabricated over a large area using this method, SERS sensors reported in this work could be practically adopted in a clinical setting as single-use disposable devices and make it possible to provide an additional verification at the point of care to help avert IV medication errors and prevent harm to patients.

Acknowledgements

The authors thank the staff of the Micro and Nanotechnology Laboratory and the Center for Nanoscale Chemical-Electrical-Mechanical Manufacturing Systems (Nano-CEMMS) at the University of Illinois at Urbana-Champaign. This work was supported by the National Science Foundation under Award No. CBET 07-54122 and ECCS 09-24062, and by Baxter Corporation. Any opinions, findings, and conclusions or recommendations expressed in this material are those of the author(s) and do not necessarily reflect the views of the National Science Foundation. The authors declare no competing financial interests.

Notes and references

^a Department of Electrical and Computer Engineering, Micro and Nanotechnology Laboratory, University of Illinois at Urbana-Champaign, 208 North Wright Street, Urbana, IL 61801, USA.

^b Department of Bioengineering, Micro and Nanotechnology Laboratory, University of Illinois at Urbana-Champaign, 208 North Wright Street, Urbana, IL 61801, USA. Email: becunningham@illinois.edu

† Electronic Supplementary Information (ESI) available: Fabrication of PNA substrates, fabrication details of the flow cell, details of FDTD simulation, characterization of the scattering volume, and detection of diltiazem diluted in DI water and PBS. See DOI: 10.1039/b000000x/

1. K. Wilson and M. Sullivan, *American Journal of Health-System Pharmacy*, 2004, **61**, 177-183.
2. S. H. Danello, R. R. Maddox and G. J. Schaack, *Hospital Pharmacy*, 2009, **44**, 680-687.
3. P. J. Schneider, Measuring medication safety with smart IV systems, San Diego, CA, 2004.
4. H. Y. Wu, W. Zhang, P. C. Mathias and B. T. Cunningham, *Nanotechnology*, 2010, **21**, 125203.
5. P. C. Mathias, S. I. Jones, H. Y. Wu, F. Yang, N. Ganesh, D. O. Gonzalez, G. Bollero, L. O. Vodkin and B. T. Cunningham, *Anal Chem*, 2010, **82**, 6854-6861.
6. S. George, I. D. Block, S. I. Jones, P. C. Mathias, V. Chaudhery, P. Vuttipittayamongkol, H. Y. Wu, L. O. Vodkin and B. T. Cunningham, *Anal Chem*, 2010, **82**, 8551-8557.
7. E. C. Le Ru, L. C. Schroeter and P. G. Etchegoin, *Anal Chem*, 2012, **84**, 5074-5079.
8. M. Fleischmann, P. J. Hendra and A. J. Mcquilla, *Chem Phys Lett*, 1974, **26**, 163-166.
9. D. L. Jeanmaire and R. P. Van Duyne, *Journal of Electroanalytical Chemistry and Interfacial Electrochemistry*, 1977, **84**, 1-20.
10. M. G. Albrecht and J. A. Creighton, *Journal of the American Chemical Society*, 1977, **99**, 5215-5217.

11. N. G. Greeneltch, M. G. Blaber, A. I. Henry, G. C. Schatz and R. P. Van Duyne, *Anal Chem*, 2013, **85**, 2297-2303.
12. H. Im, K. C. Bantz, N. C. Lindquist, C. L. Haynes and S. H. Oh, *Nano Letters*, 2010, **10**, 2231-2236.
13. A. W. Clark and J. M. Cooper, *Advanced materials*, 2010, **22**, 4025-4029.
14. M. Jin, H. van Wolferen, H. Wormeester, A. van den Berg and E. T. Carlen, *Nanoscale*, 2012, **4**, 4712-4718.
15. L. Zhang, X. Lang, A. Hirata and M. Chen, *ACS Nano*, 2011, **5**, 4407-4413.
16. C. J. Choi, H. Y. Wu, S. George, J. Weyhenmeyer and B. T. Cunningham, *Lab on a chip*, 2012, **12**, 574-581.
17. S. M. Adams, S. Campione, J. D. Caldwell, F. J. Bezares, J. C. Culbertson, F. Capolino and R. Ragan, *Small*, 2012, **8**, 2239-2249.
18. H. Y. Wu, C. J. Choi and B. T. Cunningham, *Small*, 2012, **8**, 2878-2885.
19. A. D. McFarland, M. A. Young, J. A. Dieringer and R. P. Van Duyne, *The journal of physical chemistry. B*, 2005, **109**, 11279-11285.
20. K. R. Ackermann, T. Henkel and J. Popp, *Chemphyschem : a European journal of chemical physics and physical chemistry*, 2007, **8**, 2665-2670.
21. F. Inscore, C. Shende, A. Sengupta, H. Huang and S. Farquharson, *Applied Spectroscopy*, 2011, **65**, 1004-1008.
22. V. Rana, M. V. Canameres, T. Kubic, M. Leona and J. R. Lombardi, *Journal of forensic sciences*, 2011, **56**, 200-207.
23. S. Yavuz, N. Ayabakan, M. T. Goncu and I. A. Ozdemir, *Medical Science Monitor*, 2002, **8**, 145-150.
24. S. N. Piper, B. Kumle, W. H. Maleck, A.-H. Kiessling, A. Lehmann, K. D. Röhm, S. W. Suttner and J. Boldt, *Canadian Journal Anaesthesia*, 2003, **50**, 285-292.
25. RxList - dopamine (dopamine hydrochloride) drug. [Online]. Available: <http://www.rxlist.com/dopamine-drug.htm>.
26. M. L. McGlashen, K. L. Davis and M. D. Morris, *Anal Chem*, 1990, **62**, 846-849.
27. M. L. McGlashen, K. L. Davis and M. D. Morris, Surface enhanced Raman spectroscopy of neurotransmitters, Atlanta, Georgia (USA), 1989.
28. J. Basile, *The Journal of Clinical Hypertension*, 2004, **6**, 621-629.
29. S. A. Claas and S. P. Glasser, *Expert opinion on pharmacotherapy*, 2005, **6**, 765-776.
30. RxList - cardizem (diltiazem hydrochloride) drug. [Online]. Available: <http://www.rxlist.com/cardizem-drug.htm>.
31. L. C. Strenkoski-Nix, J. Ermer, S. DeCleene, W. Cevallos and P. R. Mayer, *American Journal of Health-system Pharmacy*, 2000, **57**, 1499-1505.
32. RxList - phenergan (promethazine) drug. [Online]. Available: <http://www.rxlist.com/phenergan-drug.htm>.
33. U.S. Food and Drug Administration: Information for healthcare professionals - Intravenous promethazine and severe tissue injury, including gangrene. [Online]. Available: <http://www.fda.gov/Drugs/DrugSafety/PostmarketDrugSafetyInformationforPatientsandProviders/DrugSafetyInformationforHealthcareProfessionals/ucm182169.htm>.
34. T. D. Shenkenberg and D. D. Von Hoff, *Annals of Internal Medicine*, 1986, **105**, 67-81.
35. I. Nabiev, A. Baranov, I. Chourpa, A. Beljebbar, G. D. Sockalingum and M. Manfait, *The Journal of Physical Chemistry*, 1995, **99**, 1608-1613.
36. J. A. Anastasopoulos, A. Soto Beobide and G. A. Voyiatzis, *Journal of Raman Spectroscopy*, 2013, **44**, 401-405.
37. H. Cho, B. R. Baker, S. Wachsmann-Hogiu, C. V. Pagba, T. A. Laurence, S. M. Lane, L. P. Lee and J. B. Tok, *Nano Letters*, 2008, **8**, 4386-4390.
38. A. Beljebbar, G. D. Sockalingum, J. F. Angiboust and M. Manfait *Applied Spectroscopy*, 1996, **50**, 148-153.
39. S. Sasic, *Pharmaceutical Applications of Raman Spectroscopy* 2007.